

Zen: Near-Optimal Sparse Tensor Synchronization for Distributed DNN Training

Zhuang Wang*, Zhaozhuo Xu*, Anshumali Shrivastava, and T. S. Eugene Ng
Rice University

Abstract

Distributed training is the de facto standard to scale up the training of Deep Neural Networks (DNNs) with multiple GPUs. The performance bottleneck of distributed training lies in communications for gradient synchronization. Recently, practitioners have observed sparsity in gradient tensors, suggesting the potential to reduce the traffic volume in communication and improve end-to-end training efficiency. Yet, the optimal communication scheme to fully leverage sparsity is still missing. This paper aims to address this gap. We first analyze the characteristics of sparse tensors in popular DNN models to understand the fundamentals of sparsity. We then systematically explore the design space of communication schemes for sparse tensors and find the optimal one. We also develop a gradient synchronization system called Zen that approximately realizes it for sparse tensors. We demonstrate that Zen can achieve up to $5.09\times$ speedup in communication time and up to $2.48\times$ speedup in training throughput compared to the state-of-the-art methods.

1 Introduction

Deep Neural Networks (DNNs) have achieved remarkable empirical performance in real-world applications, such as language processing [15, 25, 28, 35, 64] and recommendation systems [22, 38, 39]. With the ever-growing size of DNN models and training datasets, it can take weeks and even months to finish training on a single GPU. Therefore, distributed training has become the norm to accelerate DNN training with multiple GPUs [24, 30, 31, 45, 48, 54, 60].

The major efficiency bottleneck of distributed training lies in communication for gradient synchronization [4, 17, 66, 67, 72]. Recent hardware developments have greatly improved the computation efficiency of DNN training. For instance, the training efficiency of BERT [15] has been doubling every year in the past three years [37]. These advancements increase the frequency of gradient synchronization in distributed training and shift more burdens to the network. However, the

network upgrades have not kept up with computation improvements [40, 49, 50], exacerbating the tension between computation and communication.

In recent years, practitioners in the deep learning community have observed the prevalence of sparsity in DNN training [8, 9, 19, 32, 38, 68, 71]. The gradients computed for each DNN layer during training form a *tensor*. Over 98% of the gradients in a tensor can be zeros [20] and these tensors can dominate the size of DNN models. We can represent non-zero gradients with a sparse format and denote the tensor with a sparse format as a *sparse tensor*. This observation provides a great opportunity to reduce communication time if sparse tensors are transmitted for gradient synchronization.

Previous works, such as AGsparse [31], SparCML [56], and OmniReduce [18], have recognized this potential. They use various sparse formats and communication schemes for sparse tensor synchronization. However, these approaches do not fully consider the fundamental characteristics of sparsity in DNN models for their designs, resulting in suboptimal performance of communication time for gradient synchronization. The root cause is that these previous works lack an understanding of the optimal scheme for sparsity. To advance the state-of-the-art, it is essential to first revisit the fundamentals of sparsity in DNN models.

This paper comprehensively analyses the characteristics of sparse tensors. We profile the sparse tensors from popular DNN models [15, 22, 25, 35] across GPUs and iterations to gain insights into how they are related to different inputs for training. Additionally, we investigate the changes in sparse tensors before and after aggregation with varying numbers of GPUs. We also examine the locations of non-zero gradients in tensors and inspect their distributions.

We next systematically explore the design space of communication schemes to synchronize sparse tensors. To construct different schemes, we discuss four elementary dimensions that consider the communication, aggregation, partition, and balance aspects of a scheme. All existing schemes [18, 30, 31, 56] can be described by these four dimensions. We find that there exists an optimal scheme for synchronizing sparse tensors.

*Both authors contributed equally.

However, the challenge lies in achieving balanced communications among GPUs and to date, no such scheme exists.

We develop a system called Zen that approximately realizes the optimal scheme within the design space described by the four dimensions. One class of natural approach is sparsity-aware tensor partitioning, but it is inefficient due to data dependency. In contrast, Zen eliminates data dependency and achieves high efficiency by using hashing algorithms. However, a challenge with hashing algorithms is the significant information loss of gradients, resulting in reduced model accuracy. To address this challenge, we propose a hierarchical hashing algorithm that guarantees balanced communications without information loss. In addition, it can fully leverage parallel computing on GPUs to minimize the incurred computation overheads for hash operations.

We summarize our contributions as follows: 1) we conduct a comprehensive analysis of the characteristics of sparse tensors; 2) we explore the design space for communication schemes for sparse tensors synchronization, and we find the optimal scheme; 3) we propose Zen that approximately realizes the optimal scheme to achieve near-optimal communication time; and 4) we evaluate Zen and show that it achieves up to $5.09\times$ speedup in communication time and up to $2.48\times$ speedup in training throughput compared to the state-of-the-art methods [18, 56].

2 Analysis of Communication Schemes for Sparse Tensor Synchronization

2.1 Gradient Sparsity in DNN Training

The synchronization of gradient tensors from different GPUs is commonly required in distributed training. For example, in data parallelism [14, 24, 31, 60], the training dataset is partitioned among all GPUs. Since GPUs have different inputs, their generated gradient tensors will also be different and they need to synchronize gradient tensors from all GPUs to ensure model consistency. In tensor model parallelism [61], individual layers of a DNN model are partitioned over multiple GPUs. These GPUs synchronize the gradient tensors during backward propagation for the gradient computation of subsequent layers. In addition, it is common practice to train large DNN models [10, 44, 48, 59, 72] with a mix of data parallelism and other parallelism strategies, such as pipeline parallelism [23, 46], tensor model parallelism [61], and ZeRO [54, 73]. These training workloads must synchronize gradient tensors across GPUs as well.

High sparsity in gradient tensors has been widely observed in DNN training [8, 9, 38, 68]. Because the training of DNN models may focus on updating a subset of parameters instead of all of them [9, 19, 71], some of the gradient tensors in DNN models are naturally sparse, with most of the gradients being zeros. Table 1 lists the statistics of four widely deployed DNN models for both recommendation systems and language processing. Each model contains two parts: multilayer per-

ceptron (MLP) and embedding table. There are two major observations from Table 1. Firstly, the embedding tables comprise a large portion of model parameters. Secondly, these embedding tables show a significant level of sparsity in their gradient tensors. We define the *density* of a gradient tensor as the percentage of its non-zero gradient values and then provide the average density for the sparse gradient tensors in the four models. As shown in the table, gradient tensors can have only 1.06% non-zero gradients in DNN training.

If the notable sparsity can be leveraged, it can significantly reduce the traffic volume for gradient synchronization and shorten the communication time in distributed training. Previous works [18, 27, 56] have recognized this potential, but the fundamental implications of sparsity are not yet understood.

2.2 Characteristics of Sparse Tensors

In this section, we will analyze the characteristics of sparse tensors in DNN models. The original gradient tensor is in a dense format, in which the gradients of all the parameters in a DNN layer are stored.

Definition 1 (Dense tensor). *We define the original gradient tensor in a DNN layer as a dense tensor.*

When there are many parameters having zero gradients, we can also represent a gradient tensor in a sparse format. A typical realization of the sparse format is coordinate lists (COO) that store a list of non-zero gradients and a list of the corresponding indices [18, 70].

Definition 2 (Sparse tensor). *We define a gradient tensor in a sparse format as a sparse tensor.*

We assume that the size of a dense tensor G is M and its density is d_G . The network bandwidth is B and the training involves n machines. For simplicity, we assume each machine has only one GPU in this section.

C1: The overlap of sparse tensors varies. Similar to dense tensors, sparse tensors need to be aggregated during synchronization. When aggregating dense tensors, the indices of gradients from different GPUs are identical. However, due to the different batches as the input for training on different GPUs, the set of indices for non-zero gradients in a sparse tensor is unknown a priori. They can have overlaps, while how much they can overlap depends on many factors, such as the DNN model, the training dataset, and the batches. We define the overlap ratio following [65] to quantify this overlaps between two sparse tensors.

Definition 3 (The overlap ratio). *Given two sparse tensors and their sets of indices for non-zero gradients are I_1 and I_2 , respectively, their overlap ratio is defined as $\frac{|I_1 \cap I_2|}{\min\{|I_1|, |I_2|\}}$, where $|\cdot|$ is the cardinality of a set.*

Figure 1a shows the probability density function (PDF) of the overlap ratios for four DNN models. We can see that the overlap ratio in a model is approximately normally distributed and it is in a wide range. In addition, different models have different distributions of overlap ratios.

Model	Task	Dataset	MLP Gradient Size	Embedding Gradient Size	Batch Size	Density
LSTM [41]	Language Modeling	One Billion Word	20M	406M	128	1.13%
DeepFM [22]	Click-through Rate Prediction	Criteo	68M	214M	1024	2.80%
NMT [35]	Machine Translation	IWSLT 2014 De-En	31M	112M	64	2.47%
BERT [15]	Question Answering	SQuAD v1.1	86M	23M	4	1.06%

Table 1: DNN models and their training statistics. Density is the average density of embedding gradient tensors on one GPU.

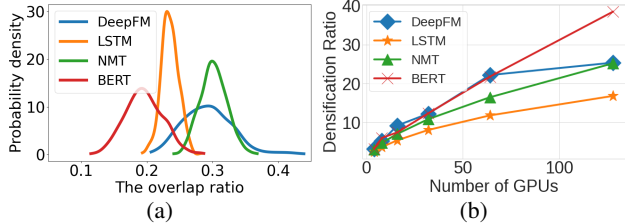


Figure 1: The characteristics of sparse tensors in DNN models. (a) shows that the overlap ratio of sparse tensors varies; (b) shows that tensors have higher density after aggregation.

C2: The tensor size after aggregation varies. When aggregating dense tensors, the tensor sizes before and after aggregation remain the same. However, when aggregating sparse tensors, the unknown overlaps of sparse tensors lead to varying tensor sizes after aggregation. Because the aggregation involves sparse tensors from multiple GPUs, we denote d_G^n as the density after the aggregation of tensors from n GPUs. We observe that sparse tensors get denser after aggregation. Here we define the densification ratio to quantify this characteristic.

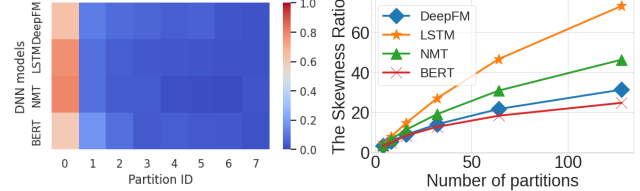
Definition 4 (The densification ratio). *Given a dense tensor G , its densification ratio is define as $\gamma_G^n = \frac{d_G^n}{d_G}$.*

Figure 1b presents the average densification ratio γ_G^n with respect to the number of GPUs for the four DNN models studied in this paper. The densification ratio increases with the number of GPUs, demonstrating that tensors have higher density after aggregation. We can also see that the densification ratio is smaller than the number of GPUs, i.e., $\gamma_G^n < n$. It suggests that the indices of non-zero gradients in sparse tensors from different GPUs are partially overlapped.

C3: The distribution of non-zero gradients is skewed. When evenly splitting a dense tensor into multiple partitions, we observe that most of the non-zero gradients are in one of them. For example, with eight partitions, over 60% of the non-zero gradients are in the first partition in the four DNN models. Figure 2a shows the percentage heatmap of the non-zero gradients in each partition for tensors from the embedding table. Here we define the skewness ratio to quantify the skewed distribution of non-zero gradients.

Definition 5 (The skewness ratio). *Given a dense tensor G and we evenly split G into n disjoint partitions, denoted as $\{G_1, \dots, G_n\}$, then the skew ratio of G with n partitions is defined as $s_G^n = \frac{\max_{i \in [n]} \{d_{G_i}\}}{d_G}$.*

Figure 2b presents the skewness ratios of gradient tensors from the embedding table in the DNN models studied in this paper. They are significant in all four models. For example, when we evenly split the gradient tensor from the embedding



(a) The heatmap of non-zero gradients distribution. (b) The skewness ratio.

Figure 2: The distribution of non-zero gradients is skewed.

table in LSTM into 128 partitions, the skewness ratio is over 70. It indicates that more than half of the non-zero gradients are in the same partition. Another observation is that the skewness ratio consistently increases with the number of partitions. It suggests that the distribution of non-zero gradients gets "skewer" with more partitions.

2.3 Performance of Communication Schemes

Communication schemes for synchronizations of dense tensors have been extensively studied [24, 30, 60, 63]. In this section, we will first explore the design space to construct communication schemes to synchronize sparse tensors for the first time. We then find the optimal schemes and conduct a numerical comparison among different schemes.

2.3.1 Elementary Dimensions for Synchronization

Given a tensor G in each GPU, the outcome of its synchronization is that gradients with the same indices are aggregated and all GPUs have identical aggregated results. We will discuss four dimensions that construct a communication scheme for the synchronizations of sparse tensors.

Communication dimension. There are typically three communication patterns for synchronization: 1) Ring, 2) Hierarchy, and 3) Point-to-point. They are illustrated in Figure 3 with an example in which there are four GPUs and GPU P_3 aggregates the data from all GPUs. In Ring, all GPUs form a ring structure. P_0 first sends its data to P_1 , which then passes the data along with its own data to P_2 and so on until P_3 receives all the data. In Hierarchy, all GPUs form a hierarchical structure and P_3 is the root. There are two stages in Figure 3b. In the first stage, P_0 sends its data to P_1 and P_2 sends its data to P_3 . In the second stage, P_1 sends the data from both its own and P_0 to P_3 . In Point-to-point communication, the other three GPUs directly send data to P_3 .

Aggregation dimension. A communication pattern can have multiple communication stages and thus there are two options for aggregation: 1) Incremental aggregation, i.e., aggregate the tensors at each communication stage; and 2) One-shot aggregation, i.e., aggregate tensors from all

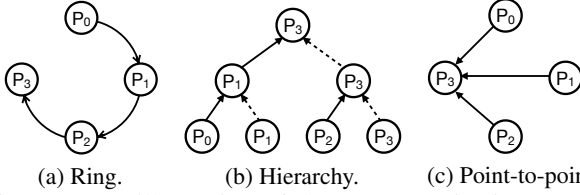


Figure 3: An illustration of three communication patterns with four GPUs. GPU P_3 aggregates the data from all GPUs.

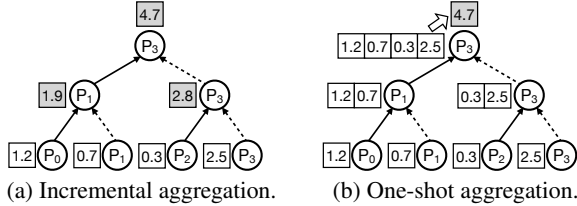


Figure 4: An illustration of two aggregation patterns with Hierarchy. The gradients on each GPU are from the same parameter and 4.7 is the final aggregated result.

GPUs after the last communication stage. In the example illustrated in Figure 3, Ring has three stages and Hierarchy has two stages. Although each GPU has one tensor for synchronization, it can host multiple tensors at each stage. Figure 4 displays an example with Hierarchy as the communication pattern. When P_1 receives a tensor from P_0 , it has two tensors due to its own tensor. P_1 can aggregate the two tensors and send the aggregated result to P_3 , as shown in Figure 4a; it can also just send the concatenated tensor to P_3 , as shown in Figure 4b. The two aggregation patterns for Point-to-point are identical because they only have one stage.

Partition dimension. There are two partition patterns to ensure that all GPUs have the same aggregated results after synchronization: 1) Centralization, in which each tensor is communicated and aggregated as a whole; and 2) Parallelism, in which each tensor is decomposed into multiple partitions and each partition is communicated and aggregated separately. Figure 5 compares the two partition patterns with Point-to-point as the communication pattern. With Centralization, as shown in Figure 5a, each GPU sends its tensor as a whole to other GPUs. With Parallelism, as shown in Figure 5b, each GPU first decomposes its tensor into three partitions and it requires two steps for synchronization. The first step aggregates the same partition from different GPUs in different places and the second step ensures that all GPUs have the aggregated results of all partitions.

Balance dimension. With Parallelism, tensors are partitioned and there are two patterns in terms of the traffic volume received at each GPU: 1) Balanced communication, in which GPUs receive the same amount of data; and 2) Imbalanced communication, in which the traffic volumes received at different GPUs are greatly different. Figure 6 compares the two balance patterns among three GPUs with Point-to-point. There are 15 gradients in the tensor and six of them are non-zero. As shown in Figure 6a, four non-zero gradients are in the middle partition and they are sent to GPU 1. The traffic

volume received at GPU 1 is $4\times$ that received at GPU 0 and GPU 2. In Figure 6b, each GPU sends two non-zero gradients to other GPUs and the volume among them is well-balanced.

The four dimensions can describe the design space of communication schemes to synchronize sparse tensors. Table 2 classifies existing schemes [18, 30, 31, 56] based on their dimensions and data formats to represent sparse tensors.

2.3.2 The Optimal Communication Schemes

We will next analyze the optimal schemes within the design space described by the four dimensions in terms of the theoretical communication time to synchronize sparse tensors.

Theorem 1 (Optimal schemes). *When choosing a communication scheme to minimize communication time:*

1. If sparse tensors exhibit little to no overlap, the scheme with Hierarchy, Incremental aggregation, and Centralization is optimal; but this case is unlikely in reality.
2. If sparse tensors are partially or fully overlapped, the optimal one is the scheme with Point-to-point, One-shot aggregation, Parallelism, and Balanced communication; this case is very likely in distributed DNN training.

Proof of Theorem 1.1. We prove it with three lemmas and the proof can be found in Appendix B.1.

Lemma 1. *When sparse tensors have no overlap, any communication scheme with Centralization can achieve this minimum with any communication pattern.*

Lemma 2. *When sparse tensors are overlapped, the scheme with Hierarchy, Incremental aggregation, and Centralization outperforms other schemes with Centralization.*

Lemma 2 implies that if we fix the choice for partition pattern to Centralization, the scheme with Hierarchy, Incremental aggregation, and Centralization is always the best.

Lemma 3. *When sparse tensors exhibit little to no overlap, the scheme with Hierarchy, Incremental aggregation, and Centralization outperforms schemes with Parallelism.*

Lemmas 1-3 imply Theorem 1.1.

Proof of Theorem 1.2. Unless otherwise specified, we assume the sparse format is COO. Communication schemes with Parallelism can suffer from imbalanced communications due to the skewed distribution of non-zero gradients. Given a dense tensor G , a straightforward parallel communication scheme first evenly splits it into multiple chunks and then extracts the non-zero gradients from each chunk. As discussed in Section 2.2, the distribution of non-zero gradients in a gradient tensor is skewed. One chunk can have much more non-zero gradients than other chunks. Consequently, one GPU has to receive most of the non-zero gradients from all the GPUs in the first step, leading to imbalanced communications among GPUs. After aggregation, the number of non-zero gradients in one GPU can be still much more than that in other GPUs. Therefore, communications in the second step are also imbalanced. It is important to note that an alternative to first extracting non-zero gradients from the gradient tensor and

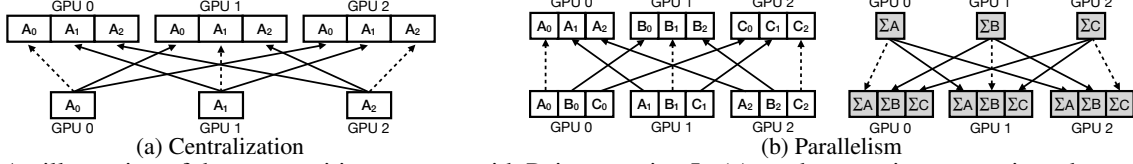


Figure 5: An illustration of the two partition patterns with Point-to-point. In (a), each tensor is communicated as a whole and each GPU receives all the tensors. In (b), each tensor is split into three partitions; the same partition from different GPUs is sent to the same place, and the aggregated results are then sent back to all GPUs.

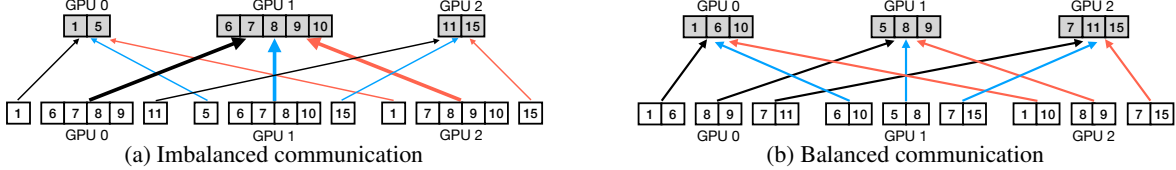


Figure 6: An illustration of the two balance patterns with Point-to-point and Parallelism. The numbers are the indices of non-zero gradients. Each GPU has six non-zero gradients. In (a), four gradients from each GPU are sent to GPU 1. In (b), each GPU sends two gradients to other GPUs, and communications among them are well-balanced. However, it is non-trivial to achieve such balanced communications.

then evenly splitting the sparse tensor into multiple partitions is not a viable option. This is because the gradients for the same parameter from different GPUs can be sent to different places, causing incomplete aggregations.

Lemma 4. *The scheme that adopts Point-to-point, One-shot aggregation, Parallelism, and Balanced communication outperforms other schemes with Parallelism.*

Lemma 4 implies that if we fix the choice for partition pattern to Parallelism, the scheme with Point-to-point, One-shot aggregation, Parallelism, and Balanced communication is always the best.

Lemma 5. *When sparse tensors are partially or fully overlapped, the scheme with Point-to-point, One-shot aggregation, Parallelism, and Balanced communication outperforms the scheme with Hierarchy, Incremental aggregation, and Centralization because the latter cannot fully leverage the overlaps among sparse tensors to minimize the traffic volume.*

Lemmas 2, 4, and 5 imply Theorem 1.2.

2.3.3 Numerical Comparison

As listed in Table 2, there are several communication schemes proposed to support the synchronizations of sparse tensors [18, 30, 31, 56]. In this section, we will compare their performance from an algorithmic perspective.

AGsparse. It adopts One-shot aggregation, Centralization, and separately collects non-zero gradients and the corresponding indices [31]. It cannot leverage the overlaps among sparse tensors to reduce the traffic volume.¹

SparCML. It adopts Hierarchical, Incremental aggregation, and Centralization [56]. According to Lemma 5, it cannot leverage the overlaps among sparse tensors to reduce the traffic volume. The performance of AGsparse and SparCML both depends on the overlaps. The fewer overlaps, the closer their performance is to the optimal. However, as shown in

¹There are different implementations for AGsparse with different communication patterns [63].

Figure 1, sparse tensors across GPUs in DNN models have significant overlaps.

Sparse PS. Parameter Servers (PS) architecture [27, 30] is a communication scheme that adopts Point-to-point, One-shot aggregation, and Parallelism. It has two roles: workers and servers. For synchronizations of sparse tensors, workers push sparse tensors to servers. After aggregation, workers pull aggregated tensors from servers to update model parameters. We call this PS architecture for sparse tensors as *Sparse PS* to distinguish it from the PS architecture for dense tensors. Because Sparse PS evenly partitions tensors, it suffers from imbalanced communications as discussed in Section 2.3.2.

OmniReduce. It also adopts Point-to-point, One-shot aggregation, and Parallelism [18]. OmniReduce consists of workers and aggregators. It splits a gradient tensor into blocks of gradients and only sends non-zero blocks, i.e., blocks with at least one non-zero gradient, to aggregators for aggregations. Compared to Sparse PS, OmniReduce does not need to transmit indices for non-zero gradients and it has a lower traffic volume for communications. However, it also requires multiple aggregators for better scalability, just like multiple servers in PS. It evenly partitions tensors and its performance also suffers from imbalanced communications.

Figure 7 numerically compares the performance of these communication schemes to synchronize sparse tensors in NMT. The sparse data formats are as each scheme proposed, i.e., OmniReduce uses tensor block; AGsparse, SparCML, and Sparse PS use COO. We only consider their theoretical communication time and ignore other overheads, such as the computation time for aggregations and the sparse tensor encoding and decoding overheads. Their communication times are normalized to *Dense*, which is the synchronization time for dense tensors².

The communication time of AGsparse linearly increases

²We use Ring-Allreduce as an example [60]. It adopts Ring, incremental aggregation, Parallelism, and Balanced communication.

Schemes	Communication	Aggregation	Partition	Balance	Note
AGsparse [31]	Ring, Hierarchy, Point-to-point	One-shot	Centralization	N/A	Cannot fully use overlaps to reduce traffic.
SparCML [56]	Hierarchy	Incremental	Centralization	N/A	
Sparse PS [30]	Point-to-point	One-shot	Parallelism	Imbalanced	Suffer from imbalanced communications.
OmniReduce [18]	Point-to-point	One-shot	Parallelism	Imbalanced	
Balanced Parallelism	Point-to-point	One-shot	Parallelism	Balanced	The optimal scheme we find.

Table 2: Comparison of different communication schemes for sparse tensors based on their dimensions.

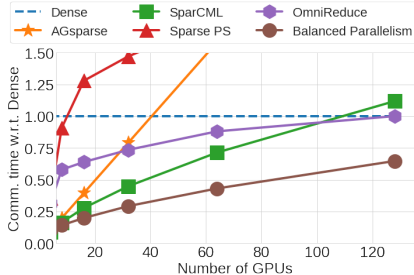


Figure 7: Comparison of different schemes for synchronizing sparse tensors in NMT [35]. The sparse data formats are as each scheme proposed, i.e., OmniReduce uses tensor block; AGsparse, SparCML, and Sparse PS use COO. For a fair comparison, the data format of Balanced Parallelism is COO.

with the number of GPUs. It performs worse than Dense with more than 40 GPUs because it does not leverage the overlaps among sparse tensors to reduce the traffic volume. Sparse PS is worse than AGsparse due to the skewed distribution of non-zero gradients and imbalanced communications among servers. It is even worse than Dense because it has to transmit both non-zero gradients and the corresponding indices. OmniReduce outperforms Dense with a small number of GPUs. However, its performance improvement is very marginal with more than 64 GPUs. Due to the skewed distribution of non-zero gradients, most of the non-zero gradients are in one partition, leading to imbalanced communications. In addition, tensors become denser after aggregation. When splitting this partition into tensor blocks (e.g., each block has 256 gradients [18]), most of them are non-zero blocks. Therefore, almost all gradients in this partition are sent to one aggregator and it becomes the communication bottleneck. SparCML is worse than Dense with a large number of GPUs due to the duplicated indices and their gradients received at each GPU.

Now, let us consider a hypothetical scheme suggested by Theorem 1 called Balanced Parallelism.

Balanced Parallelism. It adopts Point-to-point, One-shot aggregation, Parallelism, and Balanced communication. In Figure 7, we assume its sparse data format is COO for a fair comparison. Balanced Parallelism greatly outperforms existing communication schemes. For example, existing schemes cannot reduce communication time compared to Dense with 128 GPUs, but the communication time of Balanced Parallelism is still 36% lower than Dense.

Takeaways. The sparsity in DNN models offers a great opportunity to optimize communications in distributed training, but no existing schemes can fully unleash this potential. Regardless of the sparse data formats, Balanced Parallelism is opti-

mal for the common case (see Theorem 1) and thus substantially outperforms existing schemes such as SparCML [56] and OmniReduce [18]. However, no solution that realizes Balanced Parallelism exists to date. We will show how this gap is closed in the next section.

3 Zen

We propose Zen to leverage the sparsity in DNN models to minimize the synchronization time in distributed training. We first develop a hierarchical hashing algorithm to approximately achieve Balanced Parallelism. When synchronizing sparse tensors, a communication scheme with COO has to transmit non-zero gradients and their indices, which double the traffic volume. Therefore, we design a new data format for the indices to minimize the traffic volume.

3.1 Balancing Communications

3.1.1 Problem Formulation

Balanced Parallelism has the same communication pattern, aggregation pattern, and partition pattern as Sparse PS, but its communications are always well-balanced. Therefore, we borrow the concepts of workers and servers from Sparse PS to Balanced Parallelism. We also call its two communication operations as Push and Pull, respectively.

Suppose there are n workers and n servers in Balanced Parallelism. $I_i \subset \mathbb{N}_+$ is the set of indices of non-zero gradients generated by worker i . We define the problem to achieve Balanced Parallelism as follows.

Problem 1. Let I denote the union of $\{I_1, I_2, \dots, I_n\}$. We would like to have a mapping $f: I \rightarrow [n]$ such that:

1. For every $i \in [n]$ and $j \in [n]$, the cardinality of set $\{idx \in I_i | f(idx) = j\}$ is equal to $|I_i|/n$.
2. For every $j \in [n]$, the cardinality of set $\{idx \in I | f(idx) = j\}$ is equal to $|I|/n$.

Here we elaborate more on the two requirements for the mapping f accordingly as below:

1. **Load balance in Push.** For every worker, mapping f needs to decompose its non-zero gradients evenly into n partitions. Therefore, workers can transmit the same amount of non-zero gradients to each server.
2. **Load balance in Pull.** Each of the servers should have the same number of non-zero gradients after aggregation. It also implies that the same index from different workers should be sent to the same server.

Problem 1 assumes the same number of workers and servers, but it is easy to generalize this problem to cases in which the number of workers and servers are different.

3.1.2 Strawman Solutions

We will explore the opportunities for approximate solutions to Problem 1 because it is challenging to exactly solve it. Before discussing the solutions, we first define the imbalance ratio to measure the performance of algorithms to approximately solve Problem 1.

Definition 6 (The imbalance ratio). *Given a mapping f that decompose I_i into n partitions, denoted as $\{I_i^1, \dots, I_i^n\}$. The imbalance ratio of Push with f is $\max_{i,j \in [n]} \{n|I_i^j|/|I_i|\}$.*

Let I denote the union of $\{I_1, I_2, \dots, I_n\}$ and the sets of indices at the n servers after aggregation are $\{\mathbb{I}_1, \mathbb{I}_2, \dots, \mathbb{I}_n\}$. The imbalance ratio of Pull with f is $\max_{i \in [n]} \{n|\mathbb{I}_i|/|I|\}$.

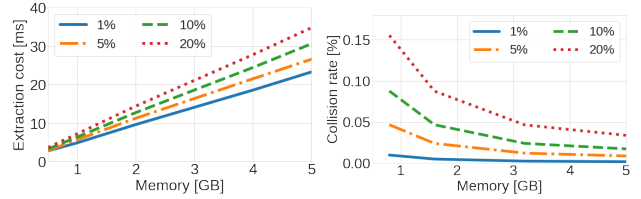
Based on Definition 6, the imbalance ratio of push in Sparse PS equals the skewness ratio, and in Balanced Parallelism is 1. Our goal is to minimize the imbalance ratio for any distributions of non-zero gradients.

Data-dependent solutions. Due to different sets of indices on different workers, data-dependent solutions need to analyze their overall distribution and calculate one mapping (see Problem 1) for all workers, inevitably incurring non-negligible computation overheads. Therefore, we cannot afford to apply a data-dependent algorithm and obtain a mapping f for every iteration. A possible approach is to compute f periodically and maintain it for the next iterations.

However, this approach can still lead to high imbalance ratios due to the varying distributions of the indices across iterations. One strawman following this approach is to sort the index set I , evenly partition it into n parts, and use the boundary indices as the thresholds to partition the index sets in the next iterations. When we compute the thresholds every 1000 iteration for NMT model [35] with $n = 16$ and apply these thresholds to the following iterations, the imbalance ratio of push fluctuates between 1.4 and 5.1, causing imbalanced communications among servers. Moreover, the imbalanced communications introduced by data-dependent solutions make it hard to estimate the iteration time. Many resource scheduling mechanisms for GPU clusters assume predictable and stable iteration times for allocating resources to DNN training jobs [36, 47, 52, 53]. It is cumbersome to schedule GPU resources with fluctuating communication time.

Strawman data-independent solution. Hashing algorithms have been widely applied to address load imbalance problems in various domains, such as distributed system [26, 62] and distributed database [16, 34]. We discuss a straightforward hashing algorithm here to approximately solve Problem 1. Note that we must leverage multiple threads in GPUs to perform hash functions to reduce computation overhead.

Given a dense tensor G , the set of indices of its non-zero gradients is I . The algorithm first allocates a memory x with shape $n \times r$, where n represents the number of partitions and r is the memory size for each partition. For every $idx \in I$, it uses a given universal hash function [7] $h : \mathbb{N}_+ \rightarrow [nr]$ to generate the hash value $h(idx)$, where nr is the range of hash function



(a) The memory size vs. the cost to extract indices. (b) The memory size vs. the hash collision rate. Figure 8: Larger memory size reduces the hash collision, but it leads to higher extraction overhead.

h . Next, it writes the idx to the $(h(idx) \bmod r)$ th location in partition $\lfloor h(idx)/r \rfloor$. The hashing operation is performed in parallel to minimize the computation overhead [68]. After that, it extracts the non-zero indices from the memory of each partition and uses them to look up the corresponding gradients from G . Finally, it returns a sparse tensor for each partition and pushes them to the corresponding servers. The pseudocode is in Appendix A.

Although a universal hash function can naturally provide an approximation to Problem 1, it is a lossy operation. Two indices can be hashed to the same location, but only one index can be written into the memory and the other is overwritten, causing the information loss of gradients.

One approach to reducing the information loss is to increase the memory size, but it leads to a dilemma between the information loss and the incurred computation overhead. After writing the indices into the memory, the algorithm needs to extract the indices, which are the non-zero values in the memory. We profile the performance of the built-in `nonzero()` API in PyTorch 1.12 on NVIDIA A100 GPUs to extract the non-zero gradients of a tensor. We set the tensor size as 214M parameters, which equals the embedding table size in DeepFM, and the performance is illustrated in Figure 8a. The extraction cost is 19.2ms when the memory size is 4GB and the density is 1%; it increases to 29.1ms when the density is 20%. This extraction cost is unacceptable as the communication time of the dense tensors in DeepFM is only around 150ms with 128 GPUs and a 100Gbps network. However, reducing the memory size can cause non-negligible information loss. For example, when the memory size is 0.85GB, which equals the tensor size, the extraction cost is 5.8ms for the density of 20%, but 15.8% gradients are lost due to hash collision, as shown in Figure 8b. We will show in Section 4.2 that the information loss can harm model accuracy.

3.1.3 A Hierarchical Hashing Algorithm

We develop a novel hashing algorithm that achieves balanced communications without information loss in distributed training with negligible extraction overhead. Before introducing our algorithm, we first discuss the possible approaches.

Approach with one hash function. As discussed in Section 3.1.2, balancing communications with only one hash function can lead to significant information loss due to hash collision. One approach to address this information loss issue

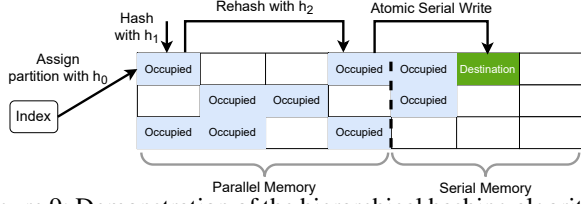


Figure 9: Demonstration of the hierarchical hashing algorithm with $n = 3$, $k = 2$, $r_1 = 4$, and $r_2 = 3$. We perform parallel hashing on the indices. For each index, we use the hash function h_0 to assign its partition. Next, we use the hash function h_1 to assign it the first location. However, because this location is occupied, we rehash it with function h_2 to the fourth location. As it is also occupied, we serially write the index into the serial memory with an atomic operation.

is to check hash collision and write all the colliding indices into a separate memory chain [55]. The hashing operation is performed in parallel, but it has to use an atomic operation to serially write the indices into the separate memory chain (denoted as *serial memory*). Otherwise, the indices in the serial memory can still be overwritten. Unfortunately, we observe that serial writing is costly when the hash collision rate is high because only one thread can operate at one time.

Approach with multiple hash functions. Another approach is to rehash a colliding index with a new hash function to another location. There is a chance that this new location is available. However, this approach can cause incomplete aggregations. Because different GPUs have different sets of indices for non-zero gradients, their sequences of indices being hashed are also different. Therefore, the location of a particular index can be different across GPUs. For example, two indices idx_1 and idx_2 , where $idx_1 < idx_2$, are hashed to the same location with the first hash function. GPU 1 has idx_2 ; GPU 2 has both idx_1 and idx_2 . In GPU 1, the location of idx_2 is determined by the first hash function, but in GPU 2, the location of idx_2 is determined by the second hash function because the location hashed by the first one has been occupied by idx_1 . Subsequently, partitioning the memory will lead to the same index assigned to different partitions at different GPUs, resulting in incomplete aggregations.

Our approach. We propose a hierarchical algorithm with multiple hash functions to guarantee complete aggregations. The first-level hash function determines the partition that an index belongs to and guarantees that an index will belong to the same partition across all GPUs. The second-level hash functions determine its locations in this partition. However, hash collision still exists even with multiple hash functions. We observe that the collision rate is less than 1% with four hash functions and the overhead to write the colliding indices into the serial memory becomes acceptable. Therefore, our approach also uses serial memory to achieve no information loss after multiple hashing.

We illustrate the hierarchical hashing algorithm in Fig-

Algorithm 1: Hierarchical Hashing Algorithm

Input: G is a dense tensor and $I \subset \mathbb{N}_+$ is a set of indices of its non-zero gradients. $n \in \mathbb{N}_+$ is the number of partitions. Each partition has memory size $r_1 + r_2$, where $r_1 \in \mathbb{N}_+$ and $r_2 \in \mathbb{N}_+$ are the memory sizes for parallel and serial operations, respectively. $h_0 : \mathbb{N}_+ \rightarrow [n]$ is a universal hash function. $H = \{h_1, \dots, h_k\}$ is a set of universal hash functions where $h_i : \mathbb{N}_+ \rightarrow [r_1]$.

Output: The partitioned sparse tensors.

```

1 Function hierarchical_hash( $I, G, h_0, H$ ):
2   Allocate memory  $x \leftarrow \mathbf{0}^{n \times (r_1 + r_2)}$ 
3   Allocate atomic counters  $c \leftarrow \mathbf{r}_1^n$ 
4   foreach  $idx \in I$  in parallel do
5      $p \leftarrow h_0(idx)$ 
6     for  $i \leftarrow 1$  to  $k + 1$  do
7        $q \leftarrow h_i(idx)$ 
8       if  $i = k + 1$  then
9          $q \leftarrow \text{atomicAdd}(c[p], 1)$ 
10         $x[p][q] \leftarrow idx$ 
11      end
12      if  $x[p][q] == 0$  then
13         $x[p][q] \leftarrow idx$ 
14        break
15      end
16    end
17  end
18   $output = []$ 
19  for  $i \leftarrow 0$  to  $n - 1$  do
20     $indices = \text{nonzero}(x[i])$ 
21     $values = G[indices]$ 
22     $output.append((indices, values))$ 
23  end
24  return  $output$ 

```

ure 9. The pseudocode of the hierarchical hashing algorithm is shown in Algorithm 1. Given a dense tensor G and the indices of its non-zero gradients I , it allocates a memory x with shape $n \times (r_1 + r_2)$, where n is the number of partitions, r_1 is the memory size for parallel hashing operations, and r_2 is the serial memory size. It performs a hashing operation for every $idx \in I$ in parallel (Lines 4-17). A universal hash function $h_0 : \mathbb{N}_+ \rightarrow [n]$ is used to locate idx to partition $p = h_0(idx)$ (Line 5). The algorithm also needs k universal hash functions $H = \{h_1, \dots, h_k\}$ with $h_i : \mathbb{N}_+ \rightarrow [r_1]$. After determining the partition p , the algorithm attempts to find an available destination $x[p][h_1(idx)]$ with h_1 . If this location is available, idx is written into it. Otherwise, the algorithm rehashes idx with h_2 to find a new location. It rehashes an index for at most k rounds and uses h_i as the hash function for round i until it finds an available destination (Lines 6-16). The algorithm writes it to the serial memory allocated to partition p after k rehashes (Lines 8-11). Serial writing is an atomic operation (Lines 9-10) to ensure no information loss. Once all indices are written into the memory, it extracts sparse tensors from the memory (Lines 19-23).

Next, we will analyze the imbalance ratio of Algorithm 1 and highlight its properties.

Guaranteed imbalance ratio. The imbalance ratio of Al-

gorithm 1 is guaranteed by the universal hash function h_0 because it determines the partition of each index.

Theorem 2 (Load Balance of Algorithm 1). *Given a dense tensor G with $|G|$ parameters. Algorithm 1 provides a mapping $f : I \rightarrow [n]$ such that*

1. *With probability at least $1 - o(1)$, its imbalance ratio of Push is at most $1 + \Theta(\sqrt{\frac{n \log n}{|G| d_G}})$.*
2. *With probability at least $1 - o(1)$, the imbalance ratio of Pull is at most $1 + \Theta(\sqrt{\frac{n \log n}{|G| d_G^m}})$.*

The proof can be found in Appendix B.2. Because $n \log n$ is orders of magnitude smaller than $|G| d_G$ and $|G| d_G^m$, Algorithm 1 performs a very good approximation to the exact solution of Problem 1 for both push and pull operations, achieving load-balanced communications among workers and servers. As shown in Section 4.3, its practical imbalance ratio is always less than 1.1 for the four DNN models we study in the paper. Note that we impose no assumptions on the data distributions and only just use the property of universal hashing defined on positive integers. Hence, Algorithm 1 can obtain a general theoretical guarantee for different distributions of non-zero gradients in DNN training.

No information loss. One may concern that two indices can be hashed to the same available location at the same time, leading to information loss. Fortunately, the probability of this special case is negligible with the probability less than 10^{-5} in our implementation on GPUs. Zen can use a write-and-read mechanism to check this collision. After memory writing, a thread reads the value stored in the memory. If the value is not what it writes, this thread takes a rehash.

Negligible extraction overhead. Thanks to multiple hashing functions and the serial memory, Algorithm 1 can achieve no information loss with a very small memory size. The incurred overhead to extract the indices from the memory after hashing (Line 20 in Algorithm 1) becomes negligible.

Strength in parallelizable computing. Because the computations for different indices are independent of each other, it enables Algorithm 1 to use multiple threads to hash and rehash them. Although the indices written in the memory are in a random order, there is no need to sort them because their orders have no effect on the aggregated results.

Hash consistency among workers. Algorithm 1 determines the partition p of each index with h_0 . To ensure that the same index from different workers can be sent to the same server, Zen allocates the same h_0 to all the workers.

3.2 Minimizing the Indices Overhead

3.2.1 Existing Sparse Formats are Inefficient

There are several sparse formats to represent sparse tensors for their synchronization. Unfortunately, none of them can minimize the overhead incurred by the indices for non-zero gradients. We assume the data type of gradients is FP32.

COO. It is efficient with a low tensor density [33, 68]. However, it doubles the traffic volume and becomes inefficient for

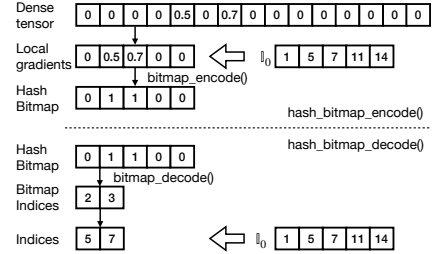


Figure 10: An illustration of the hash bitmap.

a high density. As shown in Figure 1b, tensors get denser after aggregation. For example, the average tensor density of BERT increases from 1.06% to 40.8% after the aggregation of sparse tensors from 128 GPUs. Theoretically, transmitting sparse tensors in Pull can reduce the traffic volume by $2.5\times$ compared to transmitting dense tensors, but the reduction shrinks to $1.2\times$ due to the indices for non-zero gradients.

Tensor block. It is used in OmniReduce [18]. A dense tensor is split into blocks of gradients and only non-zero blocks are transmitted. However, it is also inefficient when the tensor density is high. When splitting a tensor with high density into tensor blocks (e.g., each block has 256 gradients), most of them have at least one non-zero gradient and become non-zero tensor blocks. The communication scheme has to transit almost all the gradients.

Bitmap. It only needs one bit to indicate whether a gradient is zero or not. Unfortunately, a straightforward bitmap still incurs non-negligible traffic volume to identify non-zero gradients. When the dense tensor G is evenly partitioned, the indices of non-zero gradients in each server are in a sub-range of $[1, |G|]$, where $|G|$ is the number of gradients in G . For example, when $|G| = 15$ and there are three servers, the index range in Server i is $[5i + 1, 5(i + 1)]$. The extra bitmap size required to represent the indices of non-zero gradients in each server is $|G|/n/32$ when the data type of gradients is FP32. The total bitmap size received by each worker is constantly $|G|/32$. When the tensor size of G is 856MB, which equals the embedding table size in DeepFM, the total bitmap size is 27MB. Although Algorithm 1 enables balanced communications, the non-zero gradients in each server are randomly distributed in the whole range. If we still use a bitmap to represent the indices, the extra bitmap size in each server is $|G|/32$ and the total bitmap size received at each worker becomes $n|G|/32$, which linearly increases with the number of servers. When there are 16 servers, the total bitmap size is 428MB.

3.2.2 Hash Bitmap

We develop a *hash bitmap* for Zen to minimize the overhead to represent indices for non-zero gradients in Pull. Given a dense tensor G and h_0 in Algorithm 1, the set of indices $\mathbb{I}_i = \{idx \in [1, |G|] \mid h_0(idx) = i\}$ in each worker that should be pushed to Server i is determined, though it is not in a continuous range. Since \mathbb{I}_i and \mathbb{I}_j are disjoint when $i \neq j$, it provides an opportunity to construct the bitmap based on \mathbb{I}_i , rather than the whole range.

Algorithm 2: The hash bitmap

Input: G is a dense tensor. $\mathbb{I}_i = \{idx \in [1, |G|] \mid h_0(idx) = i\}$, where h_0 is defined in Algorithm 1.

```
1 Function hash_bitmap_encode( $G, \mathbb{I}_i$ ):  
2    $local\_gradients = G[\mathbb{I}_i]$   
3    $hash\_bitmap = \text{bitmap\_encode}(local\_gradients)$   
4   return  $hash\_bitmap$   
5 Function hash_bitmap_decode( $\mathbb{I}_i, hash\_bitmap$ ):  
6    $bitmap\_indices = \text{bitmap\_decode}(hash\_bitmap)$   
7    $indices = \mathbb{I}_i[bitmap\_indices]$   
8   return  $indices$ 
```

Figure 10 illustrates how the hash bitmap works for \mathbb{I}_0 with $|G| = 15$ and three servers. The indices for the two non-zero gradients are $\{5, 7\}$. `hash_bitmap_encode()` is used to encode the indices. Given a dense tensor G , it first extracts the local gradients according to the indices in \mathbb{I}_0 . It then encodes the local gradients into a bitmap. Because the second and the third gradients are non-zero, the second bit and the third bit in the hash bitmap are 1 and the other bits are 0. `hash_bitmap_decode()` is used to decode the hash bitmap to a set of indices. It first decodes a hash bitmap to the bitmap indices, which are the indices of 1. For example, because the second and the third bits in the hash bitmap are 1, the bitmap indices are $\{2, 3\}$. It then uses the bitmap indices as the indices to extract the corresponding values in \mathbb{I}_0 as the global indices for non-zero gradients. In this example, the values are $\{5, 7\}$, which are exactly the indices for the two non-zero gradients. The pseudocode is shown in Algorithm 2.

The function `hash_bitmap_encode()` is invoked at each server, which then broadcasts the hash bitmap to all the workers. After each worker receives the hash bitmaps from all the servers, it invokes `hash_bitmap_decode()` to decode the hash bitmaps to the indices with the corresponding \mathbb{I}_i . Note that \mathbb{I}_i is computed and sorted offline and it remains unchanged for the same h_0 in both servers and workers.

Theorem 3. *In Pull of Zen, the total hash bitmap size received at each worker from all servers is constantly $|G|/32$.*

The proof is in Appendix B.3. Zen still uses COO to represent sparse tensors in Push due to the low tensor density. The benefit of replacing COO with hash bitmap is limited.

4 Evaluation

4.1 Experimental Setup

Testbeds. There are two testbeds in the evaluation. The first testbed contains 16 GPU machines equipped with NVLink and the machines are connected by a 25Gbps network with TCP/IP. Each machine has 8 NVIDIA V100 GPUs (32 GB GPU memory) and 2 CPUs/48 cores (Intel Xeon 8260 at 2.40GHz). The second testbed contains 16 GPU machines equipped with NVLink and the machines are connected by a 100Gbps network with RDMA. Each machine has 8 NVIDIA A100 GPUs (40 GB GPU memory) and 4 CPUs/256 cores (AMD EPYC 7742 at 2.25GHz). Each machine runs Ubuntu

20.04 and the software environment includes CUDA-11.0, PyTorch-1.8.0, Horovod-0.22.1, NCCL-2.7.8, and CuPy-11.0.

Workloads. We use four popular DNN models for both recommendation systems (DeepFM [22]) and language processing (LSTM [25], NMT [35], and BERT [15]). Table 1 lists their training datasets and their batch sizes. These models can fit into the memory of each GPU. The per-GPU batch size is kept constant as the number of GPUs increases.

Baselines. We compare Zen with AGsparse [31], SparCML (SSAR_Recursive_double) [56], Sparse PS [30], and OmniReduce [18]. We use AllReduce in Horovod [60] as Dense for the synchronization of dense tensors. We also provide the upper bound on the training throughput of DNN models (Upper Bound). This is obtained by assuming the lower bound³ of the communication time can be achieved by leveraging the sparsity in DNN models.

Implementation. We implement the hierarchical hash algorithm in CUDA and then use it as an extension for PyTorch. The hash function we use in Algorithm 1 is MurmurHash [1]. We only need to set the seeds for MurmurHash to generate different hash functions. At the beginning of training, Zen generates a set of random seeds and then broadcasts the seeds to all the GPUs to ensure that they have the same set of hash functions in Algorithm 1. Because NVLink is equipped in GPU machines, Zen communicates dense tensors within machines with ReduceScatter/AllGather [21, 63].

4.2 End-to-end Experiments

In this section, we present the end-to-end training efficiency of Zen on the four models and compare it with the baselines. We set $k = 3$, $r_1 = 2|G|d_G$, and $r_2 = r_1/10$ for Algorithm 1.

Training throughput improvement. Figure 11 shows the results with a 25Gbps TCP/IP network. Zen outperforms all baselines by processing more samples in a second. In LSTM model, the best baseline is SparCML. Zen achieves up to $1.67\times$ speedup over SparCML, $2.48\times$ speedup over OmniReduce, and $3.1\times$ speedup over AllReduce in the end-to-end training throughput. In both DeepFM and NMT with 16 machines, the best baseline is OmniReduce. Zen achieves $1.44\times$ speedup and $1.51\times$ speedup over OmniReduce for DeepFM and NMT, respectively. The performance of Zen for BERT is very close to the upper bound; it achieves $1.13\times$ speedup over AllReduce and $1.07\times$ speedup over OmniReduce. As we increase the number of machines, the benefits of Zen over SparCML and OmniReduce are enlarged, indicating Zen’s great scalability. When we increase the network bandwidth from 25Gbps to 100Gbps, Zen still has great end-to-end speedups, as shown in Figure 12. Specifically, in LSTM model, Zen achieves up to $1.50\times$ speedup over SparCML, which is the best baseline. In DeepFM and NMT, Zen

³For any GPU involved in training, it must receive non-zero gradients in G from all other GPUs during synchronization. The overall density of sparse tensors from other $n - 1$ GPUs after aggregation is d_G^{n-1} . The lower bound of communication time is $d_G^{n-1}M/B$, without transmitting the indices.

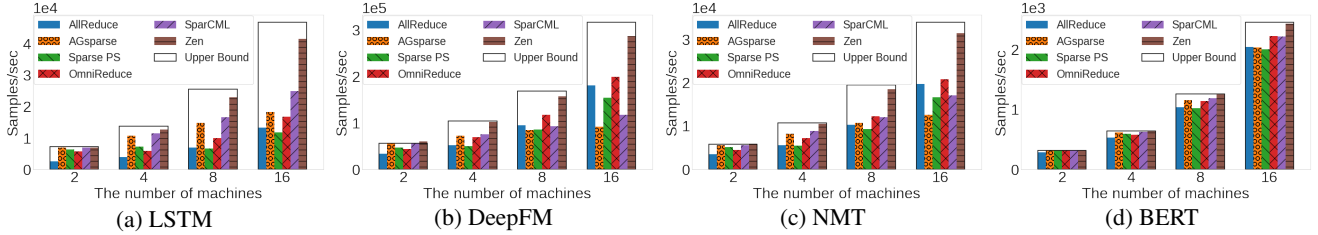


Figure 11: Training throughput of DNN models with 25Gbps TCP/IP networks.

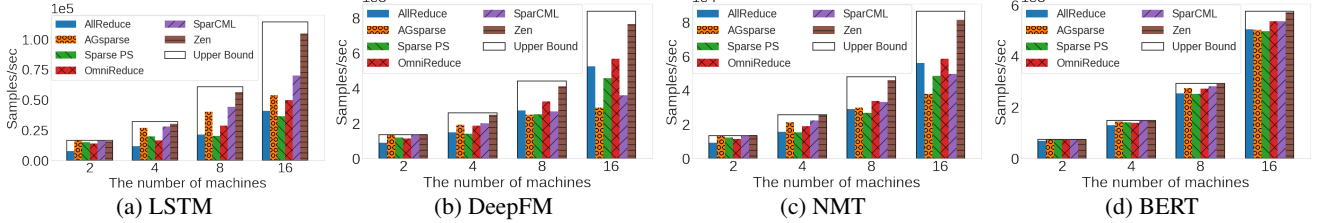


Figure 12: Training throughput of DNN models with 100Gbps RDMA networks.

achieves up to $1.46\times$ and $1.45\times$ speedups over AllReduce and up to $1.34\times$ and $1.39\times$ speedups over the best baseline OmniReduce. These results demonstrate that Zen fully leverages sparsity in DNN models to optimize training efficiency.

Communication improvement. The performance of Zen is driven by the reduction in communication time. Figure 13 shows the speedups of different communication schemes compared to AllReduce with 16 machines and a 25Gbps network. The speedup of OmniReduce is up to $1.58\times$. We observe the performance of AGsparse, Sparse PS, and SparCML can be even worse than AllReduce in some cases. They use COO as the sparse format. The communication time of AGsparse linearly increases with the number of machines. Sparse PS has severe imbalanced communications and it has to transmit both gradients and indices. With a high density, the sparse tensor size with COO is larger than the dense tensor size. With SparCML, the overlaps among sparse tensors can be received multiple times at each GPU. In contrast, Zen achieves $6.77\times$ speedup for LSTM and $3.0\times$ speedup for BERT. Its speedups over SparCML and OmniReduce are up to $2.82\times$ and $5.09\times$, respectively. Zen also achieves $2.10\times$ speedup for DeepFM and $1.97\times$ speedup for NMT.

Model accuracy. We will demonstrate that Zen can preserve the iteration-wise accuracy of DNN models as AllReduce because there is no information loss in Algorithm 1. We also take the strawman data-independent solution (refer to Section 3.1.2) as a baseline. It can achieve balanced communications at the cost of information loss due to hash collision, which is related to the used auxiliary memory size. Given a dense tensor $|G|$ with the density d_G , the memory size used in Zen is $2|G|d_G$. We vary the memory size in the strawman to evaluate the impacts on accuracy with different information loss rates. Figure 14 displays the test accuracy of DeepFM with different schemes. Zen and AllReduce have the same iteration-wise accuracy during training. When the memory size is $2|G|$ in the strawman (denoted as $2|G|$ Strawman in

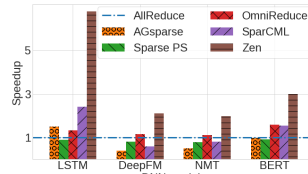


Figure 13: Communication speedups for embedding gradients in the four DNN models compared to AllReduce.

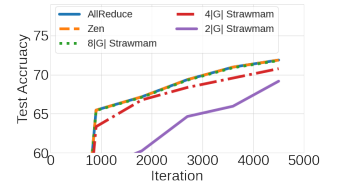


Figure 14: DeepFM Accuracy speedups for embedding gradients in the four DNN models compared to AllReduce. We set the strawman with different memory sizes.

Figure 14), the information loss rate is around 9% and the training accuracy has a noticeable drop compared to training with AllReduce. Increasing the memory size to $8|G|$ (denoted as $8|G|$ Strawman) can reduce the rate to around 1% and it almost has no harm on the accuracy. However, it can lead to costly overhead to extract the indices from the memory. The communication time is around 60ms, but the extraction overhead is around 45ms with A100 GPUs. In contrast, the extraction overhead in Zen after hashing is only around 2ms thanks to the small memory size.

4.3 Microbenchmarks

Guaranteed load balance. Figure 15 presents the imbalance ratio of DeepFM using Sparse PS and Zen, respectively. Figure 15a shows that the imbalance ratio of Push with Sparse PS is severe due to the skewed distribution of non-zero gradients and it gets worse with more machines. It leads to imbalanced communications among servers and one of the servers has to receive most of the non-zero gradients. Similarly, the imbalance ratio of Pull with Sparse PS is also very high. In contrast, applying Zen can significantly reduce the imbalance ratio in both Push and Pull. Zen can always keep the imbalance ratio smaller than 1.1, regardless of the number of machines, as shown in Figure 15b. This conclusion is consistent across different DNN models. It demonstrates that Zen guarantees well-balanced communications in distributed training.

A study on parameters for Algorithm 1. We simulate a

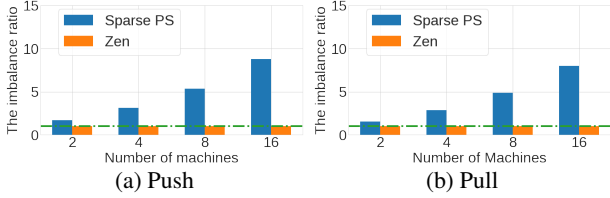


Figure 15: The imbalance ratio of DeepFM in Pull and Push.

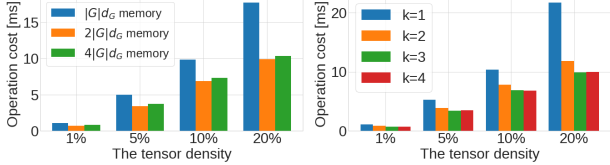


Figure 16: The computation overhead of Algorithm 1.

tensor with size 214M (same as the embedding gradients in DeepFM) and vary its density to perform a study on both r_1 and k in Algorithm 1. We first study parameter r_1 . We set $r_2 = r_1/10$ and $k = 3$. As shown in Figure 16a, when we increase r_1 from $|G|d_G$ to $2|G|d_G$, there is a notable reduction in the operation cost because the larger memory size increases the probability of successful parallel writing and reduces the workload of serial writing. But when we further increase r_1 from $2|G|d_G$ to $4|G|d_G$, it leads to a higher computation time. There are two reasons behind this effect. Firstly, the workload of serial writing is already low with $2|G|d_G$ memory. Further increasing r_1 only marginally helps reduce the computation overhead. Secondly, a larger memory size can increase the computation overhead to extract the indices (see Algorithm 1) and thus degrades the overall performance. Figure 16b shows the computation costs versus k when we use $2|G|d_G$ memory. Increasing k from 1 to 3 can help reduce the operation cost as it alleviates the serial writing workload, but $k = 3$ and $k = 4$ have very similar operation costs.

The hash bitmap. We demonstrate the effectiveness of the hash bitmap to represent the indices of non-zero gradients. Figure 17 shows the tensor data size with different sparse formats. The sizes are normalized to the dense tensor and there are 16 servers. The tensor density is the total density of all servers after aggregation. The gap between the hash bitmap and COO increases with the tensor density. It also significantly outperforms the bitmap. In addition, the hash bitmap can still reduce the traffic volume with a density of 95% compared to the dense tensor, but the bitmap and COO cannot save the volume when the density is greater than 50%. The performance of tensor blocks varies with the distribution of non-zero gradients. For some sparse tensors in the four DNN models we study, it can even transmit higher traffic volume than COO because a non-zero block has more zero gradients than non-zero gradients.

Zen’s performance breakdown. We also break down the performance of Zen by Algorithm 1 and the hash bitmap format. Figure 18 illustrates the speedup breakdown over AllReduce with 16 machines and a 25Gbps network. It can be

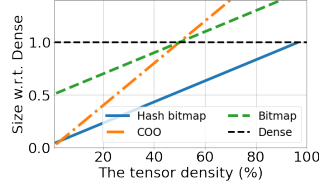


Figure 17: The effectiveness of the hash bitmap.

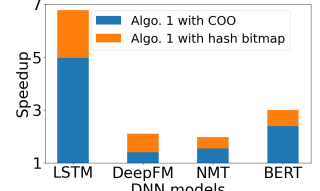


Figure 18: The performance breakdown of Zen.

seen that the primary performance benefits of Zen come from Algorithm 1, with the hash bitmap format providing noticeable additional benefits. For example, when the data format is COO after applying Algorithm 1, the speedup is $4.97\times$ and $2.39\times$ for LSTM and BERT, respectively. Replacing COO with the hash bitmap can further improve the speedups by 36% and 26%.

5 Related Work

Related work on schemes to support sparse tensors synchronization has already been discussed in Section 2.3.3.

Acceleration of dense tensor synchronization. ATP [29] and SwitchML [58] exploit programmable switches for the synchronization of dense tensors. BytePS [24] uses spare CPU and bandwidth resources in GPU clouds to optimize communications. These approaches disregard the values of gradients and communicate all gradients. In contrast, Zen leverages sparsity in DNN models and only transmits non-zero gradients to reduce the synchronization time.

Acceleration of sparse tensor synchronization. Parallax [27] utilizes Sparse PS and it cannot achieve balanced communications in synchronization. Zen can achieve balanced communications by using a novel hierarchical hashing algorithm. Flare [13] and Libra [51] use programmable switches to accelerate sparse tensor communications, but they rely on specific hardware. Moreover, Zen analyzes the characteristics of sparse tensors and explores the design space for communication schemes to determine the optimal one, but prior approaches did not consider these factors.

Hash algorithms for load balancing. Previous works have attempted to achieve load balancing using hashing [3, 5, 6, 11, 69]. They typically assign two partitions to a given index using two hash functions and then selecting the partition with more available memory as the final destination [12, 42, 43, 57]. However, these methods require serial writing of indices to memory and cannot leverage the parallel computing power of GPUs. In contrast, Zen enables parallelizable computing on GPUs. While DRAGONN [68] introduces a hash-based algorithm for parallel writing of non-zero gradients to memory, it does not address the imbalanced communications in distributed training and cannot handle hash collisions, resulting in information loss. In contrast, Zen achieves balanced communications and avoids information loss.

6 Conclusion

In summary, we systematically explore the design space to identify the optimal communication scheme for sparse tensor synchronization in distributed training. Our realization of this scheme, Zen, is data-independent and includes a novel hashing algorithm that can use parallel computing on GPUs to achieve well-balanced communications among GPUs without information loss.

References

- [1] Austin Appleby. Murmurhash 2.0, 2008.
- [2] Ammar Ahmad Awan, Ching-Hsiang Chu, Hari Subramoni, and Dhableswar K Panda. Optimized broadcast for deep learning workloads on dense-GPU InfiniBand clusters: MPI or NCCL? In *Proceedings of the 25th European MPI Users' Group Meeting*, pages 1–9, 2018.
- [3] Yossi Azar, Andrei Z Broder, Anna R Karlin, and Eli Upfal. Balanced allocations. In *Proceedings of the twenty-sixth annual ACM symposium on theory of computing*, pages 593–602, 1994.
- [4] Youhui Bai, Cheng Li, Quan Zhou, Jun Yi, Ping Gong, Feng Yan, Ruichuan Chen, and Yinlong Xu. Gradient compression supercharged high-performance data parallel DNN training. In *Proceedings of the ACM SIGOPS 28th Symposium on Operating Systems Principles*, pages 359–375, 2021.
- [5] Petra Berenbrink, Artur Czumaj, Angelika Steger, and Berthold Vöcking. Balanced allocations: The heavily loaded case. *SIAM Journal on Computing*, 35(6):1350–1385, 2006.
- [6] Zhiruo Cao, Zheng Wang, and Ellen Zegura. Performance of hashing-based schemes for internet load balancing. In *Proceedings IEEE INFOCOM 2000. Conference on Computer Communications. Nineteenth Annual Joint Conference of the IEEE Computer and Communications Societies (Cat. No. 00CH37064)*, volume 1, pages 332–341. IEEE, 2000.
- [7] J Lawrence Carter and Mark N Wegman. Universal classes of hash functions. In *Proceedings of the ninth annual ACM symposium on Theory of computing*, pages 106–112, 1977.
- [8] Beidi Chen, Zichang Liu, Binghui Peng, Zhaozhuo Xu, Jonathan Lingjie Li, Tri Dao, Zhao Song, Anshumali Shrivastava, and Christopher Re. MONGOOSE: A learnable LSH framework for efficient neural network training. In *International Conference on Learning Representations (ICLR)*, 2021.
- [9] Beidi Chen, Tharun Medini, James Farwell, Charlie Tai, Anshumali Shrivastava, et al. Slide: In defense of smart algorithms over hardware acceleration for large-scale deep learning systems. *Proceedings of Machine Learning and Systems*, 2:291–306, 2020.
- [10] Aakanksha Chowdhery, Sharan Narang, Jacob Devlin, Maarten Bosma, Gaurav Mishra, Adam Roberts, Paul Barham, Hyung Won Chung, Charles Sutton, Sebastian Gehrmann, et al. PaLM: Scaling language modeling with pathways. *arXiv preprint arXiv:2204.02311*, 2022.
- [11] Artur Czumaj, Chris Riley, and Christian Scheideler. Perfectly balanced allocation. In *Approximation, Randomization, and Combinatorial Optimization.. Algorithms and Techniques*, pages 240–251. Springer, 2003.
- [12] Søren Dahlgaard, Mathias Bæk Tejs Knudsen, Eva Rotenberg, and Mikkel Thorup. The power of two choices with simple tabulation. In *Proceedings of the twenty-seventh annual ACM-SIAM symposium on Discrete algorithms*, pages 1631–1642. SIAM, 2016.
- [13] Daniele De Sensi, Salvatore Di Girolamo, Saleh Ashkboos, Shigang Li, and Torsten Hoefler. Flare: Flexible in-network allreduce. In *Proceedings of the International Conference for High Performance Computing, Networking, Storage and Analysis*, pages 1–16, 2021.
- [14] Jeffrey Dean, Greg Corrado, Rajat Monga, Kai Chen, Matthieu Devin, Mark Mao, Marc’ aurelio Ranzato, Andrew Senior, Paul Tucker, Ke Yang, Quoc Le, and Andrew Ng. Large scale distributed deep networks. In *Advances in Neural Information Processing Systems (NIPS)*, 2012.
- [15] Jacob Devlin, Ming-Wei Chang, Kenton Lee, and Kristina Toutanova. BERT: pre-training of deep bidirectional transformers for language understanding. In *Proceedings of the 2019 Conference of the North American Chapter of the Association for Computational Linguistics: Human Language Technologies, NAACL-HLT 2019, Minneapolis, MN, USA, June 2-7, 2019, Volume 1 (Long and Short Papers)*, pages 4171–4186, 2019.
- [16] Carla Schlatter Ellis. Extendible hashing for concurrent operations and distributed data. In *Proceedings of the 2nd ACM SIGACT-SIGMOD Symposium on Principles of Database Systems*, pages 106–116, 1983.
- [17] Jiawei Fei, Chen-Yu Ho, Atal N Sahu, Marco Canini, and Amedeo Sapio. Efficient sparse collective communication and its application to accelerate distributed deep learning. In *Proceedings of the 2021 ACM SIGCOMM 2021 Conference*, pages 676–691, 2021.

- [18] Jiawei Fei, Chen-Yu Ho, Atal N Sahu, Marco Canini, and Amedeo Sapio. Efficient sparse collective communication and its application to accelerate distributed deep learning. In *Proceedings of the 2021 ACM SIGCOMM 2021 Conference*, pages 676–691, 2021.
- [19] Jonathan Frankle and Michael Carbin. The lottery ticket hypothesis: Finding sparse, trainable neural networks. In *International Conference on Learning Representations*, 2018.
- [20] Trevor Gale, Erich Elsen, and Sara Hooker. The state of sparsity in deep neural networks. *arXiv preprint arXiv:1902.09574*, 2019.
- [21] William Gropp. Mpich2: A new start for mpi implementations. In *European Parallel Virtual Machine/Message Passing Interface Users’ Group Meeting*, pages 7–7. Springer, 2002.
- [22] Huifeng Guo, Ruiming Tang, Yunming Ye, Zhenguo Li, and Xiuqiang He. Deepfm: a factorization-machine based neural network for ctr prediction. In *Proceedings of the 26th International Joint Conference on Artificial Intelligence*, pages 1725–1731, 2017.
- [23] Yanping Huang, Youlong Cheng, Ankur Bapna, Orhan Firat, Dehao Chen, Mia Chen, Hyoungho Lee, Jiquan Ngiam, Quoc V Le, Yonghui Wu, et al. Gpipe: Efficient training of giant neural networks using pipeline parallelism. *Advances in neural information processing systems*, 32:103–112, 2019.
- [24] Yimin Jiang, Yibo Zhu, Chang Lan, Bairen Yi, Yong Cui, and Chuanxiong Guo. A unified architecture for accelerating distributed DNN training in heterogeneous GPU/CPU clusters. In *14th {USENIX} Symposium on Operating Systems Design and Implementation OSDI 20*, pages 463–479, 2020.
- [25] Rafal Jozefowicz, Oriol Vinyals, Mike Schuster, Noam Shazeer, and Yonghui Wu. Exploring the limits of language modeling. *arXiv preprint arXiv:1602.02410*, 2016.
- [26] David Karger, Eric Lehman, Tom Leighton, Rina Panigrahy, Matthew Levine, and Daniel Lewin. Consistent hashing and random trees: Distributed caching protocols for relieving hot spots on the world wide web. In *Proceedings of the twenty-ninth annual ACM symposium on Theory of computing*, pages 654–663, 1997.
- [27] Soojeong Kim, Gyeong-In Yu, Hojin Park, Sungwoo Cho, Eunji Jeong, Hyeonmin Ha, Sanha Lee, Joo Seong Jeong, and Byung-Gon Chun. Parallax: Sparsity-aware data parallel training of deep neural networks. In *Proceedings of the Fourteenth EuroSys Conference 2019*, pages 1–15, 2019.
- [28] Ryan Kiros, Yukun Zhu, Russ R Salakhutdinov, Richard Zemel, Raquel Urtasun, Antonio Torralba, and Sanja Fidler. Skip-thought vectors. In *Advances in neural information processing systems*, pages 3294–3302, 2015.
- [29] ChonLam Lao, Yanfang Le, Kshiteej Mahajan, Yixi Chen, Wenfei Wu, Aditya Akella, and Michael M Swift. Atp: In-network aggregation for multi-tenant learning. In *NSDI*, pages 741–761, 2021.
- [30] Mu Li, David G Andersen, Jun Woo Park, Alexander J Smola, Amr Ahmed, Vanja Josifovski, James Long, Eugene J Shekita, and Bor-Yiing Su. Scaling distributed machine learning with the parameter server. In *USENIX Symposium on Operating Systems Design and Implementation (OSDI)*, 2014.
- [31] Shen Li, Yanli Zhao, Rohan Varma, Omkar Salpekar, Pieter Noordhuis, Teng Li, Adam Paszke, Jeff Smith, Brian Vaughan, Pritam Damania, et al. Pytorch distributed: Experiences on accelerating data parallel training. *Proceedings of the VLDB Endowment*, 13(12).
- [32] Shengwei Li, Zhiquan Lai, Dongsheng Li, Yiming Zhang, Xiangyu Ye, and Yabo Duan. Embrace: Accelerating sparse communication for distributed training of deep neural networks. In *Proceedings of the 51st International Conference on Parallel Processing*, pages 1–11, 2022.
- [33] Yujun Lin, Song Han, Huizi Mao, Yu Wang, and William J Dally. Deep gradient compression: Reducing the communication bandwidth for distributed training. *The International Conference on Learning Representations (ICLR)*, 2017.
- [34] Witold Litwin, Marie-Anne Neimat, and Donovan A Schneider. Lh*—a scalable, distributed data structure. *ACM Transactions on Database Systems (TODS)*, 21(4):480–525, 1996.
- [35] Minh-Thang Luong, Hieu Pham, and Christopher D Manning. Effective approaches to attention-based neural machine translation. In *Proceedings of the 2015 Conference on Empirical Methods in Natural Language Processing*, pages 1412–1421, 2015.
- [36] Kshiteej Mahajan, Arjun Balasubramanian, Arjun Singhvi, Shivaram Venkataraman, Aditya Akella, Amar Phanishayee, and Shuchi Chawla. Themis: Fair and efficient GPU cluster scheduling. In *17th USENIX Symposium on Networked Systems Design and Implementation (NSDI 20)*, pages 289–304, 2020.
- [37] Peter Mattson, Christine Cheng, Gregory Diamos, Cody Coleman, Paulius Micikevicius, David Patterson, Hanlin Tang, Gu-Yeon Wei, Peter Bailis, Victor Bittorf, et al.

- MLperf training benchmark. *Proceedings of Machine Learning and Systems*, 2:336–349, 2020.
- [38] Tharun Medini, Beidi Chen, and Anshumali Shrivastava. Solar: Sparse orthogonal learned and random embeddings. In *International Conference on Learning Representations*, 2020.
- [39] Tharun Kumar Reddy Medini, Qixuan Huang, Yiqiu Wang, Vijai Mohan, and Anshumali Shrivastava. Extreme classification in log memory using count-min sketch: A case study of amazon search with 50m products. *Advances in Neural Information Processing Systems*, 32, 2019.
- [40] Mellanox. Mellanox Corporate Update. https://www.mellanox.com/related-docs/company/MLNX_Corporate_Deck.pdf, 2022.
- [41] Stephen Merity, Nitish Shirish Keskar, and Richard Socher. Regularizing and optimizing lstm language models. *arXiv preprint arXiv:1708.02182*, 2017.
- [42] Michael Mitzenmacher. The power of two choices in randomized load balancing. *IEEE Transactions on Parallel and Distributed Systems*, 12(10):1094–1104, 2001.
- [43] Michael Mitzenmacher and Eli Upfal. *Probability and computing: Randomization and probabilistic techniques in algorithms and data analysis*. Cambridge university press, 2017.
- [44] Dheevatsa Mudigere, Yuchen Hao, Jianyu Huang, Zhihao Jia, Andrew Tulloch, Srinivas Sridharan, Xing Liu, Mustafa Ozdal, Jade Nie, Jongsoo Park, et al. Software-hardware co-design for fast and scalable training of deep learning recommendation models. In *Proceedings of the 49th Annual International Symposium on Computer Architecture*, pages 993–1011, 2022.
- [45] Deepak Narayanan, Aaron Harlap, Amar Phanishayee, Vivek Seshadri, Nikhil R Devanur, Gregory R Ganger, Phillip B Gibbons, and Matei Zaharia. PipeDream: generalized pipeline parallelism for DNN training. In *Proceedings of the 27th ACM Symposium on Operating Systems Principles*, pages 1–15, 2019.
- [46] Deepak Narayanan, Aaron Harlap, Amar Phanishayee, Vivek Seshadri, Nikhil R Devanur, Gregory R Ganger, Phillip B Gibbons, and Matei Zaharia. PipeDream: Generalized pipeline parallelism for DNN training. In *Proceedings of the 27th ACM Symposium on Operating Systems Principles*, pages 1–15, 2019.
- [47] Deepak Narayanan, Keshav Santhanam, Fiodar Kazhamiaka, Amar Phanishayee, and Matei Zaharia. {Heterogeneity-Aware} cluster scheduling policies for deep learning workloads. In *14th USENIX Symposium on Operating Systems Design and Implementation (OSDI 20)*, pages 481–498, 2020.
- [48] Deepak Narayanan, Mohammad Shoeybi, Jared Casper, Patrick LeGresley, Mostofa Patwary, Vijay Korthikanti, Dmitri Vainbrand, Prethvi Kashinkunti, Julie Bernauer, Bryan Catanzaro, et al. Efficient large-scale language model training on GPU clusters using Megatron-LM. In *Proceedings of the International Conference for High Performance Computing, Networking, Storage and Analysis*, pages 1–15, 2021.
- [49] NVIDIA. A Timeline of Innovation for NVIDIA. <https://www.nvidia.com/en-us/about-nvidia/corporate-timeline/>, 2021.
- [50] OpenAI. AI and Compute. <https://openai.com/blog/ai-andcompute/>, 2021.
- [51] Heng Pan, Penglai Cui, Zhenyu Li, Ru Jia, Penghao Zhang, Leilei Zhang, Ye Yang, Jiahao Wu, Jianbo Dong, Zheng Cao, Qiang Li, Hongqiang Harry Liu, Mathy Laurent, and Gaogang Xie. Enabling fast and flexible distributed deep learning with programmable switches. *arXiv preprint arXiv:2205.05243*, 2022.
- [52] Yanghua Peng, Yixin Bao, Yangrui Chen, Chuan Wu, and Chuanxiong Guo. Optimus: an efficient dynamic resource scheduler for deep learning clusters. In *Proceedings of the Thirteenth EuroSys Conference*, pages 1–14, 2018.
- [53] Aurick Qiao, Sang Keun Choe, Suhas Jayaram Subramanya, Willie Neiswanger, Qirong Ho, Hao Zhang, Gregory R Ganger, and Eric P Xing. Pollux: Co-adaptive cluster scheduling for goodput-optimized deep learning. In *15th {USENIX} Symposium on Operating Systems Design and Implementation ({OSDI} 21)*, 2021.
- [54] Samyam Rajbhandari, Jeff Rasley, Olatunji Ruwase, and Yuxiong He. ZeRO: Memory optimizations toward training trillion parameter models. In *SC20: International Conference for High Performance Computing, Networking, Storage and Analysis*, pages 1–16. IEEE, 2020.
- [55] M Ramakrishna, E Fu, and E Bahcekapili. A performance study of hashing functions for hardware applications. In *Proc. of Int. Conf. on Computing and Information*, pages 1621–1636. Citeseer, 1994.
- [56] Cédric Renggli, Saleh Ashkboos, Mehdi Aghagolzadeh, Dan Alistarh, and Torsten Hoefler. Sparcml: High-performance sparse communication for machine learning. In *Proceedings of the International Conference for High Performance Computing, Networking, Storage and Analysis*, pages 1–15, 2019.

- [57] Andrea W Richa, M Mitzenmacher, and R Sitaraman. The power of two random choices: A survey of techniques and results. *Combinatorial Optimization*, 9:255–304, 2001.
- [58] Amedeo Sapia, Marco Canini, Chen-Yu Ho, Jacob Nelson, Panos Kalnis, Changhoon Kim, Arvind Krishnamurthy, Masoud Moshref, Dan Ports, and Peter Richtarik. Scaling distributed machine learning with {In-Network} aggregation. In *18th USENIX Symposium on Networked Systems Design and Implementation (NSDI 21)*, pages 785–808, 2021.
- [59] Teven Le Scao, Angela Fan, Christopher Akiki, Ellie Pavlick, Suzana Ilić, Daniel Hesslow, Roman Castagné, Alexandra Sasha Luccioni, François Yvon, Matthias Gallé, et al. BLOOM: A 176B-parameter open-access multilingual language model. *arXiv preprint arXiv:2211.05100*, 2022.
- [60] Alexander Sergeev and Mike Del Balso. Horovod: fast and easy distributed deep learning in tensorflow. *arXiv preprint arXiv:1802.05799*, 2018.
- [61] Mohammad Shoeybi, Mostofa Patwary, Raul Puri, Patrick LeGresley, Jared Casper, and Bryan Catanzaro. Megatron-lm: Training multi-billion parameter language models using model parallelism. *arXiv preprint arXiv:1909.08053*, 2019.
- [62] Ion Stoica, Robert Morris, David Karger, M Frans Kaashoek, and Hari Balakrishnan. Chord: A scalable peer-to-peer lookup service for internet applications. *ACM SIGCOMM computer communication review*, 31(4):149–160, 2001.
- [63] Rajeev Thakur, Rolf Rabenseifner, and William Gropp. Optimization of collective communication operations in MPICH. *The International Journal of High Performance Computing Applications*, 19(1), 2005.
- [64] Ashish Vaswani, Noam Shazeer, Niki Parmar, Jakob Uszkoreit, Llion Jones, Aidan N Gomez, Łukasz Kaiser, and Illia Polosukhin. Attention is all you need. In *Advances in neural information processing systems*, pages 5998–6008, 2017.
- [65] MK Vijaymeena and K Kavitha. A survey on similarity measures in text mining. *Machine Learning and Applications: An International Journal*, 3(2):19–28, 2016.
- [66] Zhuang Wang, Haibin Lin, Yibo Zhu, and T. S. Eugene Ng. Hi-speed DNN training with espresso: Unleashing the full potential of gradient compression with near-optimal usage strategies. In *Proceedings of the Eighteenth European Conference on Computer Systems*, pages 867–882, 2023.
- [67] Zhuang Wang, Xinyu Wu, Zhaozhao Xu, and T. S. Eugene Ng. Cupcake: A compression scheduler for scalable communication-efficient distributed training. *Proceedings of Machine Learning and Systems*, 5, 2023.
- [68] Zhuang Wang, Zhaozhao Xu, Xinyu Wu, Anshumali Shrivastava, and T. S. Eugene Ng. Dragonn: Distributed randomized approximate gradients of neural networks. In *International Conference on Machine Learning*, pages 23274–23291. PMLR, 2022.
- [69] Udi Wieder et al. Hashing, load balancing and multiple choice. *Foundations and Trends® in Theoretical Computer Science*, 12(3–4):275–379, 2017.
- [70] Hang Xu, Chen-Yu Ho, Ahmed M Abdelmoniem, Aritra Dutta, El Houcine Bergou, Konstantinos Karatsenidis, Marco Canini, and Panos Kalnis. Grace: A compressed communication framework for distributed machine learning. In *Proc. of 41st IEEE Int. Conf. Distributed Computing Systems (ICDCS)*, 2021.
- [71] Haoran You, Chaojian Li, Pengfei Xu, Yonggan Fu, Yue Wang, Xiaohan Chen, Richard G Baraniuk, Zhangyang Wang, and Yingyan Lin. Drawing early-bird tickets: Toward more efficient training of deep networks. In *International Conference on Learning Representations, 2019*, 2020.
- [72] Zhen Zhang, Shuai Zheng, Yida Wang, Justin Chiu, George Karypis, Trishul Chilimbi, Mu Li, and Xin Jin. MiCS: Near-linear scaling for training gigantic model on public. *Proceedings of the VLDB Endowment*, 16(1):37–50, 2022.
- [73] Yanli Zhao, Andrew Gu, Rohan Varma, Liang Luo, Chien-Chin Huang, Min Xu, Less Wright, Hamid Shojanazeri, Myle Ott, Sam Shleifer, et al. PyTorch FSDP: experiences on scaling fully sharded data parallel. *arXiv preprint arXiv:2304.11277*, 2023.

Appendix

A Algorithm for a Strawman Solution

In this section, we present Algorithm 3, which is the algorithm for the data-independent solution with a naive hashing algorithm. This algorithm supplements the discussions in Section 3.1.2.

B Theoretical Analysis

B.1 Proof of Theorem 1

Theorem 1 (Optimal schemes). *When choosing a communication scheme to minimize communication time:*

Algorithm 3: A strawman solution with hashing

Input: G is a dense tensor and $I \subset \mathbb{N}_+$ is a set of indices of its non-zero gradients. $n \in \mathbb{N}_+$ is the number of partitions. $r \in \mathbb{N}_+$ is the memory size for each partition. $h: \mathbb{N}_+ \rightarrow [nr]$ is an universal hash function.

Output: The partitioned sparse tensors.

```
1 Function Main( $I, G, h(\cdot)$ ):  
2   Allocate memory  $x \leftarrow \mathbf{0}^{n \times r}$   
3   foreach  $idx \in I$  in parallel do  
4      $p \leftarrow \lfloor h(idx)/r \rfloor$   
5      $q \leftarrow h(idx) \bmod r$   
6      $x[p][q] \leftarrow idx$   
7   end  
8    $output = []$   
9   for  $i \leftarrow 0$  to  $n - 1$  do  
10     $indices = \text{nonzero}(x[i])$   
11     $values = G[indices]$   
12     $output.append((indices, values))$   
13  end  
14  return  $output$ ;
```

1. If sparse tensors exhibit little to no overlap, the scheme with Hierarchy, Incremental aggregation, and Centralization is optimal; but this case is unlikely in reality.
2. If sparse tensors are partially or fully overlapped, the optimal one is the scheme with Point-to-point, One-shot aggregation, Parallelism, and Balanced communication; this case is very likely in distributed DNN training.

Proof of Theorem 1.1. We prove it with three lemmas. When any two sparse tensors have no overlaps, the minimum traffic volume each GPU has to receive is all the tensors from other GPUs. Any communication scheme with Centralization achieves the optimal communication time. Therefore, we have the following lemma.

Lemma 1. *When sparse tensors have no overlap, any communication scheme with Centralization can achieve this minimum with any communication pattern.*

When sparse tensors are overlapped, we have the following lemmas.

Lemma 2. *When sparse tensors are overlapped, the scheme with Hierarchy, Incremental aggregation, and Centralization outperforms other schemes with Centralization.*

Proof. Let n denote the number of GPUs and I_0, I_1, \dots, I_{n-1} are the set of indices for non-zero gradients in each GPU, respectively. C is the overlap of all the sparse tensors, i.e., $C = \bigcap I_i$. If a communication scheme adopts point-to-point communication or one-shot aggregation, each GPU has to receive C for $n - 1$ times. Then we consider Incremental aggregation and the communication pattern is Ring or Hierarchy. With Ring, the tensor from each GPU is aggregated at each stage and then forwarded to the next GPU. Consequently, this tensor is received by every GPU. Because C is the common overlap, each GPU also has to receive C for $n - 1$ times. When the communication pattern is Hierarchy, each GPU receives data from all the other GPUs with its own hierarchical structure that has $\log n + 1$ levels, as shown in Figure 3b. Because

the root GPU is in each level, it has to receive C for $\log n$ times. It suggests that the traffic volume in the scheme with Hierarchy, Incremental aggregation, and Centralization is less than that in other schemes with Centralization. Let C' denote the overlap of a subset of the sparse tensors, we can have a similar conclusion that a subset of GPUs has to receive C' multiple times. In other words, each GPU still has to receive the overlaps multiple times. \square

Lemma 2 implies that if we fix the choice for partition pattern to Centralization, the scheme with Hierarchy, Incremental aggregation, and Centralization is always the best.

Lemma 3. *When sparse tensors exhibit little to no overlap, the scheme with Hierarchy, Incremental aggregation, and Centralization outperforms schemes with Parallelism.*

Proof. For schemes with Parallelism, the aggregation operation in their first step aims to reduce the traffic volume in the second step when sparse tensors overlap. But when sparse tensors exhibit little to no overlap, or minimal overlap at best, the first step has no benefits and the communication time in the second step equals the communication time of schemes with Centralization. It implies that schemes with Parallelism have longer communication time than schemes with Centralization. \square

Lemmas 1-3 imply Theorem 1.1.

Proof of Theorem 1.2. Unless otherwise specified, we assume the sparse format is COO. Communication schemes with Parallelism can suffer from imbalanced communications due to the skewed distribution of non-zero gradients. Given a dense tensor G , a straightforward parallel communication scheme first evenly splits it into multiple chunks and then extracts the non-zero gradients from each chunk. As discussed in Section 2.2, the distribution of non-zero gradients in a gradient tensor is skewed. One chunk can have much more non-zero gradients than other chunks. Consequently, one GPU has to receive most of the non-zero gradients from all the GPUs in the first step, leading to imbalanced communications among GPUs. After aggregation, the number of non-zero gradients in one GPU can be still much more than that in other GPUs. Therefore, communications in the second step are also imbalanced. It is important to note that an alternative to first extracting non-zero gradients from the gradient tensor and then evenly splitting the sparse tensor into multiple partitions is not a viable option. This is because the gradients for the same parameter from different GPUs can be sent to different places, causing incomplete aggregations.

Lemma 4. *The scheme that adopts Point-to-point, One-shot aggregation, Parallelism, and Balanced communication outperforms other schemes with Parallelism.*

Proof. There are three communication patterns: Ring, Hierarchy, and Point-to-point. We first consider communication

schemes with Point-to-point communication and Parallelism, namely, the PS architecture. Given a gradient tensor G with the density of d_G and there are n servers. We first analyze the communication time of push and pull operations separately. We then discuss the communication time of different PS schemes.

Push. Because the skewness ratio is s_G^n , the largest density in the n partitions is $s_G^n d_G$. The size of the sparse tensor extracted from this partition is $2s_G^n d_G M/n$. As a result, the communication time of push in sparse PS is $2(n-1)s_G^n d_G M/n/B$.

Pull. After aggregation, the largest density in the n partitions becomes $s_G^n d_G^n$. In existing implementations of the PS architecture, the communication time of Pull is $2(n-1)s_G^n d_G^n M/n/B$ because each server needs to broadcast its aggregated results to all the workers with point-to-point communications [24, 30]. In theory, there are other ways to implement Pull in the PS architecture. For example, each server can perform a broadcast collective operation. The performance of broadcast with different algorithms is analyzed in [2] and its communication time for Pull can be expressed as $2bd_G^n M/B$, where b is the number of rounds in an algorithm. For example, $b = \lceil \log n \rceil$ when it uses Binomial Tree Algorithm and $b = \frac{2(n-1)}{n}$ when it uses Scatter-AllGather Algorithm [2, 21].

Sparse PS. Combining the communication time of push and pull with point-to-point communications, its overall communication time is $2(n-1)(d_G + d_G^n)s_G^n M/n/B$.

Sparse PS with the broadcast. When considering broadcast for Pull, the overall communication time becomes $2(n-1)s_G^n d_G M/n/B + 2bd_G^n M/B$. We denote this case as sparse PS with the broadcast.

For simplicity, we call the scheme with Point-to-point, One-shot aggregation, Parallelism, and Balanced communication as Balanced Parallelism.

Balanced Parallelism. In Balanced Parallelism, the skewness ratio s_G^n is always 1. We replace the s_G^n in the communication time of sparse PS as 1 and have the communication time for Balanced Parallelism: $2(n-1)(d_G + d_G^n)M/n/B$.

Balanced Parallelism is optimal among schemes with Parallelism. It is clear that Balanced Parallelism is much better than sparse PS when the skewness ratio is large DNN models. The performance ratio of PS with broadcast to Balanced Parallelism is $\frac{s_G^n}{1+\gamma_G^n} + \frac{n}{n-1} \frac{b\gamma_G^n}{1+\gamma_G^n} > \frac{s_G^n + b\gamma_G^n}{1+\gamma_G^n}$. Because both s_G^n and b are greater than 1, the ratio is also greater than 1. Hence, Balanced Parallelism always outperforms sparse PS and sparse PS with broadcast in terms of communication time. \square

Lemma 4 implies that if we fix the choice for partition pattern to Parallelism, the scheme with Point-to-point, One-shot aggregation, Parallelism, and Balanced communication is always the best.

Lemma 5. *When sparse tensors are partially or fully overlapped, the scheme with Point-to-point, One-shot aggregation, Parallelism, and Balanced communication outperforms the*

scheme with Hierarchy, Incremental aggregation, and Centralization because the latter cannot fully leverage the overlaps among sparse tensors to minimize the traffic volume.

Proof. Because One-shot aggregation cannot leverage the overlaps among sparse tensors, the performance of communication schemes with One-shot aggregation is worse than those with Incremental aggregation. Therefore, we only consider Incremental aggregation for schemes with Ring communication or Hierarchy communication. We consider the best case for them, i.e., the skewness ratio is 1 after tensor partition with Parallelism. In addition, we only need to compare the first step because they have the same communication time in the second step. The communication time of the first step in Balanced Parallelism is $2(n-1)d_G M/n/B$.

Schemes with Ring and Incremental Aggregation. They have $n-1$ communication stages. The tensor density in the i_{th} stage is d_G^i . Note that $d_G^1 = d_G$. Therefore, the communication time is $2\sum_{i=1}^{n-1} d_G^i M/n/B$. Because tensors can get denser after aggregation, we have $d_G^i \leq d_G^j$ when $i < j$ and $\sum_{i=1}^{n-1} d_G^i \geq (n-1)d_G$. As a result, the communication time of schemes with Ring and Incremental aggregation is no less than that of Balanced Parallelism.

Schemes with Hierarchy and Incremental aggregation. They have $\log n$ communication stages. Because each partition has a hierarchical structure, the total traffic volume in the i_{th} stage is $\frac{d_G^{2^{i-1}}}{2^{i-1}} Mn$ and the total traffic volume in all the $\log n$ stages is $V = \sum_{i=1}^{\log n} \frac{d_G^{2^{i-1}}}{2^{i-1}} Mn$. Because $d_G^{2^{i-1}} \geq d_G$, we have $V \geq \sum_{i=1}^{\log n} \frac{d_G}{2^{i-1}} Mn = 2(n-1)d_G M$. Therefore, the traffic volume received at each GPU is no less than $2(n-1)d_G M/n$ and the communication time is no less than that of Balanced Parallelism. \square

In summary, Balanced Parallelism outperforms other PS schemes and the performance of other schemes with Parallelism cannot be better than Balanced Parallelism. Lemmas 2, 4, and 5 imply Theorem 1.2.

B.2 Proof of Theorem 2

Theorem 2 (Load Balance of Algorithm 1). *Given a dense tensor G with $|G|$ parameters. Algorithm 1 provides a mapping $f: I \rightarrow [n]$ such that*

1. *With probability at least $1 - o(1)$, its imbalance ratio of push is at most $1 + \Theta(\sqrt{\frac{n \log n}{|G|d_G}})$.*
2. *With probability at least $1 - o(1)$, the imbalance ratio of pull is at most $1 + \Theta(\sqrt{\frac{n \log n}{|G|d_G^n}})$.*

Proof. The imbalance ratio of Algorithm 1 is only determined by $h_0: \mathbb{N}_+ \rightarrow [n]$, while the hash function set H focuses on exact memory write.

The number of indices in I_i is $|G|d_G$, where d_G is the density of G . Since h_0 is data-independent, part 1 in Problem 1

can be formulated as: given $|G|d_G$ balls, we would like to toss them into n bins with the universal hash function h_0 . Taking the results from [3], the maximum load of the bins is at most $\frac{|G|d_G}{n} + \Theta(\sqrt{|G|d_G \log n/n})$ with probability at least $1 - o(1)$. Recall the definition of the imbalance ratio of push in Definition 6:

$$Push_{h_0}^n = \max_{i,j \in [n]} \frac{n|I_i^j|}{|I_i|}.$$

Because $\max\{|I_i^j|\} \leq \frac{|G|d_G}{n} + \Theta(\sqrt{|G|d_G \log n/n})$, we have

$$\begin{aligned} Push_{h_0}^n &\leq \frac{|G|d_G + \Theta(\sqrt{|G|d_G n \log n})}{|G|d_G} \\ &= 1 + \Theta\left(\sqrt{\frac{n \log n}{|G|d_G}}\right), \end{aligned}$$

with probability at least $1 - o(1)$. Thus, we finish the proof of the first part.

Since h_0 is data-independent, part 2 in Problem 1 can be formulated as: given $|I| = |G|d_G^n$ balls, we would like to toss them into n bins with the universal hash function h_0 . The maximum load of the bins is at most $\frac{|G|d_G^n}{n} + \Theta(\sqrt{|G|d_G^n \log n/n})$ with probability at least $1 - o(1)$. Recall the definition of the imbalance ratio of pull in Definition 6:

$$Pull_{h_0}^n = \max_{i \in [n]} \frac{n|I_i|}{|I|}.$$

Because $\max\{|I_i|\} \leq \frac{|G|d_G^n}{n} + \Theta(\sqrt{|G|d_G^n \log n/n})$, we have

$$\begin{aligned} Pull_{h_0}^n &\leq \frac{|G|d_G^n + \Theta(\sqrt{|G|d_G^n n \log n})}{|G|d_G^n} \\ &= 1 + \Theta\left(\sqrt{\frac{n \log n}{|G|d_G^n}}\right), \end{aligned}$$

with probability at least $1 - o(1)$. Thus, we finish the proof of the second part. \square

B.3 Proof of Theorem 3

Theorem 3. *In Pull of Zen, the total hash bitmap size received at each worker from all servers is constantly $|G|/32$.*

Proof. Suppose there are n servers. The set of indices that should be pushed to Server i is $\mathbb{I}_i = \{idx \in [1, |G|] \mid h_0(idx) = i\}$. With `hash_bitmap_encode()`, the size of the hash bitmap encoded at Server i is $|\mathbb{I}_i|/32$. Because each worker needs to receive the hash bitmap from all the servers, the total size is $\sum_{i=0}^{n-1} |\mathbb{I}_i|/32 = |G|/32$. \square